Physics of Fluids

Analysis of droplet clustering in air-assist sprays using Voronoi tessellations

Cite as: Phys. Fluids **30**, 123305 (2018); https://doi.org/10.1063/1.5053473
Submitted: 23 August 2018 . Accepted: 26 November 2018 . Published Online: 26 December 2018

Manish M, and Srikrishna Sahu

View Online Export Citation CrossMark

ARTICLES YOU MAY BE INTERESTED IN

Time resolved measurements of droplet preferential concentration in homogeneous isotropic turbulence without mean flow
Physics of Fluids **31**, 025103 (2019); https://doi.org/10.1063/1.5063673

Coalescence dynamics of unequal sized drops
Physics of Fluids **31**, 012105 (2019); https://doi.org/10.1063/1.5064516

Rising dynamics and lift effect in dense segregating granular flows
Physics of Fluids **30**, 123303 (2018); https://doi.org/10.1063/1.5045576

© 2018 Author(s).

Analysis of droplet clustering in air-assist sprays using Voronoi tessellations

Manish M and Srikrishna Sahu[a)]
Department of Mechanical Engineering, IIT Madras, Chennai, India

(Received 23 August 2018; accepted 26 November 2018; published online 26 December 2018)

A comprehensive understanding on the dynamics of droplet clustering in sprays is important for a wide range of applications ranging from combustion engines to spray drying. Due to inherent flow inhomogeneity and air entrainment, the mechanism of dispersion of droplets in sprays is not the same as that in homogeneous and isotropic turbulence, which has been relatively well studied. The current research work aims to understand the physics of clustering of polydispersed water droplets in air-assist sprays. In particular, the focus is on studying the influence of local liquid mass loading on droplet clustering in the spray. For this purpose, the injector was operated for different inlet air and water flow rates. The droplet clusters as well as voids were uniquely characterized by the application of the Voronoi analysis on the spray images captured using the particle image velocimetry technique far downstream of the injector exit. The interferometric laser imaging for droplet sizing technique was used to measure the droplet size distribution. The droplet clustering in the spray was found to be a multi-scale process that spans over a wide range, from tens of the Kolmogorov scale up to a fraction of spray half-width. Similar normalized distributions of cluster and void areas for different cases suggested self-similarity of the clustering process. A new method for characterizing the length scale of droplet clusters was described. The average cluster length scale and the degree of clustering were found to strongly depend on local liquid mass fraction and gas phase Reynolds number. The radial evolution of droplet cluster statistics across the spray was also examined. *Published by AIP Publishing.* https://doi.org/10.1063/1.5053473

I. INTRODUCTION

Understanding preferential concentration and/or clustering of particles in particle-laden turbulent flows has gained a lot of interest among various researchers since the past few decades due to its relevance to many environmental and industrial processes such as pollutant dispersion, cloud formation, spray drying, and combustion (Balachandar and Eaton, 2010). It is well known that particles with Stokes number (ratio of particle time constant to some turbulence time scale) of the order of "one" tend to preferentially accumulate in highly strained and low vorticity regions of the carrier phase flow (see Maxey, 1987; Fessler *et al.*, 1994; Sundaram and Collins, 1999; and Ferrante and Elghobashi, 2003, to name a few). Clustering refers to the case when the extent of particle accumulation and segregation is such that locally dense and almost empty regions are created. Although clusters of particles evolve dynamically, the group of particles within a cluster remains close to each other for time scales comparable to turbulent time scales of the carrier phase flow (Monchaux *et al.*, 2012). Hence, clustering can lead to strong spatio-temporal inhomogeneity in the particle concentration field that can be of important concern. For example, in fuel spray combustion, the droplet evaporation rate in locally dense regions is significantly reduced due to droplet clustering which subsequently influences the process of air-fuel mixture preparation (Sahu *et al.*, 2018a) and heat release rate and flame stability (Chiu and Liu, 1977; Akamatsu *et al.*, 1996; and Hardalupas *et al.*, 1994). Smith *et al.* (2002) found that the size and location of particle clusters affect the ignition phenomena in pulverized coal flames. In spray drying processes, the preferential accumulation of droplets can modify the drying kinetics of individual droplets (Lampa and Fritsching, 2013). Close spacing of droplets within clusters has been observed to strongly influence dynamics and drag on the individual droplets (Manish and Sahu, 2019 and Razzaghi *et al.*, 2018). Considering that most flows in nature and practical applications contain particles with a broad size distribution, characterization of clusters in polydisperse systems is of utmost importance. The present research work aims to examine droplet clustering in polydispersed isothermal sprays based on experimental characterization of individual clusters of droplets within the spray. Throughout the text, "particles" refer to the dispersed medium in two-phase flows in general, while "droplets" refer to the liquid particles in sprays.

In the past, several experimental studies reported preferential accumulation of particles/droplets in homogeneous and isotropic turbulent flows which can be broadly classified into two categories: (a) experiments in a "turbulence box," where zero-mean flow is realized (Wood *et al.*, 2005; Yang and Shy, 2005; and Lian, 2014) and (b) grid-generated turbulence in wind tunnels (Aliseda *et al.*, 2002; Saw *et al.*, 2008; Monchaux *et al.*, 2010; Sumbekova *et al.*, 2017; and Obligado *et al.*, 2011). While some of the above studies considered mono-sized particles, dispersion of relatively wider particle size distribution has also been reported, especially in

[a)]Electronic mail: ssahu@iitm.ac.in

the wind-tunnel based studies. The above studies discussed not only the physics of clustering in detail but also different approaches to characterize clusters. However, the mechanism of dispersion of droplets in a spray can be considerably different from that in isotropic turbulence. Apart from the presence of a wide range of droplet sizes, which interact with a broad range of turbulent eddies of the air flow, the inherent flow inhomogeneity and the air entrainment into a spray strongly influence the dispersion of droplets. Due to momentum and energy exchange between the dispersed and the carrier phases, the turbulence characteristics of the entrained air flow into the spray and downstream of the injector exit depend on the inlet fluid flow rate into the injector. In spite of earlier attempts to characterize droplet clusters in sprays under isothermal conditions (Heinlein and Fritsching, 2006; Sahu *et al.*, 2016; and Zimmer and Ikeda, 2003), evaporating conditions (Sahu *et al.*, 2018a), and reacting environment (McDonell *et al.*, 1992; Akamatsu *et al.*, 1996; and Sornek and Dobashi, 2000), droplet clustering in sprays is not yet well understood. According to some of the recent studies (Sumbekova *et al.*, 2017 and Obligado *et al.*, 2011) pertaining to droplet dispersion in isotropic turbulence, the clustering of droplets has been found to be a multi-scale process although numerical studies (Squires and Eaton, 1990; Boivin *et al.*, 1998; Sundaram and Collins, 1999; and Ferrante and Elghobashi, 2003, to name a few) emphasize the role of small scale eddies of the carrier phase flow. However, the studies on free shear flows observed strong influence of large scale eddies on particle clustering (Longmire and Eaton, 1992 and Sahu *et al.*, 2014). As far as sprays are concerned, it is not yet clear if droplet clustering is a multi-scale process and in such cases if the role of large or small scale eddies is important. In addition, there are several points that need attention: How does the droplet concentration within the clusters vary according to the size of the clusters? Should the geometric characteristics of the clusters depend on their size? Also, importantly, how does local liquid mass loading influence clustering (although the role of Stokes number on preferential accumulation of particles has been widely studied, the influence of local particle loading is not yet well understood) and if there exists a spatial preference within a spray for clustering of droplets. In order to comment on the above aspects, statistical characterization of droplet clusters is not enough; rather, identification of individual clusters is crucial. Although several approaches are available for characterizing particle clusters (see Saw *et al.*, 2008 and Monchaux *et al.*, 2012 for a review on this topic), the approach based on the calculation of Voronoi tessellations has been found to be satisfactory for identifying individual particle clusters (Monchaux *et al.*, 2010; Sumbekova *et al.*, 2017; Obligado *et al.*, 2014; 2015; García-Villalba *et al.*, 2012; Nilsen *et al.*, 2013; Soldati and Marchioli, 2012; and Tagawa *et al.*, 2013). The Voronoi analysis has the unique advantage of providing the instantaneous cluster distribution map, which is beneficial for a quantitative study on clustering including geometric characterization of droplet clusters.

The present paper attempts to address the important issues on droplet clustering in sprays as outlined above based on the optical measurement of droplets in laboratory scale air-assist sprays in conjunction with Voronoi analysis of the spray images. In the past, only few studies considered droplet clustering in air-assist atomizers in spite of their practical importance (for instance, Heinlein and Fritsching, 2006; Sahu *et al.*, 2016; 2018a; and Ficuciello *et al.*, 2017). In the present experiments, the droplet measurements are obtained at far downstream locations of the injector and across the spray. At these locations, the preferential accumulation of droplets is expected due to interaction of spray droplets with the surrounding air flow rather than owing to the liquid breakup phenomenon, which is important close to the injector exit. In addition, this allows identification of individual droplets on the spray images, which is essential for calculation of the Voronoi diagrams. Experiments are performed for four injector operating conditions that allow studying droplet clustering for a range of local liquid mass loading. The droplet clusters are characterized and also the degree of clustering is quantified for each injector operating condition and radial measurement station across the spray.

Section II describes the experimental setup and the image processing details. It also includes a brief description of the method of the Voronoi analysis and our approach for geometric characterization of the droplet clusters. Section III discusses the experimental results with emphasis on the effect of local liquid mass loading on droplet clustering. The spatial variation of droplet cluster characteristics and the degree of clustering across the spray are also reported. The main findings are summarized in Sec. IV.

II. EXPERIMENTAL SETUP AND IMAGE PROCESSING

A. Flow arrangement and instrumentation

A schematic of the experimental setup is shown in Fig. 1. An internal mixing type air assist atomizer (Spraying system Co. 1/4 J series) was used to produce a solid cone water spray under ambient atmospheric conditions. The atomizer receives compressed air and pressurized water from a pressure vessel through separate inlets. The flow rates of air and water were measured and regulated using respective flowmeters and control valves. The spray was injected into open atmosphere and was devoid of any external acoustic perturbations (Ficuciello *et al.*, 2017 and Yang and Turan, 2017). The injector was operated under four different operating flow conditions, as shown in Table I, corresponding to different volume flow rates of water (Q_l) for the same volume flow rate of air (Q_a) and vice versa. The droplet measurements were taken 30 cm downstream of the injector exit such that the droplet number density is not too high and the probability of droplet-droplet interaction leading to coalescence or breakup is low. The local liquid mass fraction (ϕ_m) was estimated based on the measurement of average droplet number density and velocity and characteristic droplet size as per the following equation:

$$\phi_m = \frac{\alpha \overline{U} \rho_l}{\alpha \overline{U} \rho_l + \overline{U_g} \rho_g}, \tag{1}$$

where α is the liquid volume loading ratio ($\alpha = \overline{N}(\pi(VMD)^3/6)$), $\overline{N}$ is the average droplet number density, VMD is the volume mean diameter ($=\left(\frac{\sum_{i=1}^{n} D_i}{n}\right)^{1/3}$, where n is the total number of droplets), $\overline{U}$ and $\overline{U_g}$ are the average

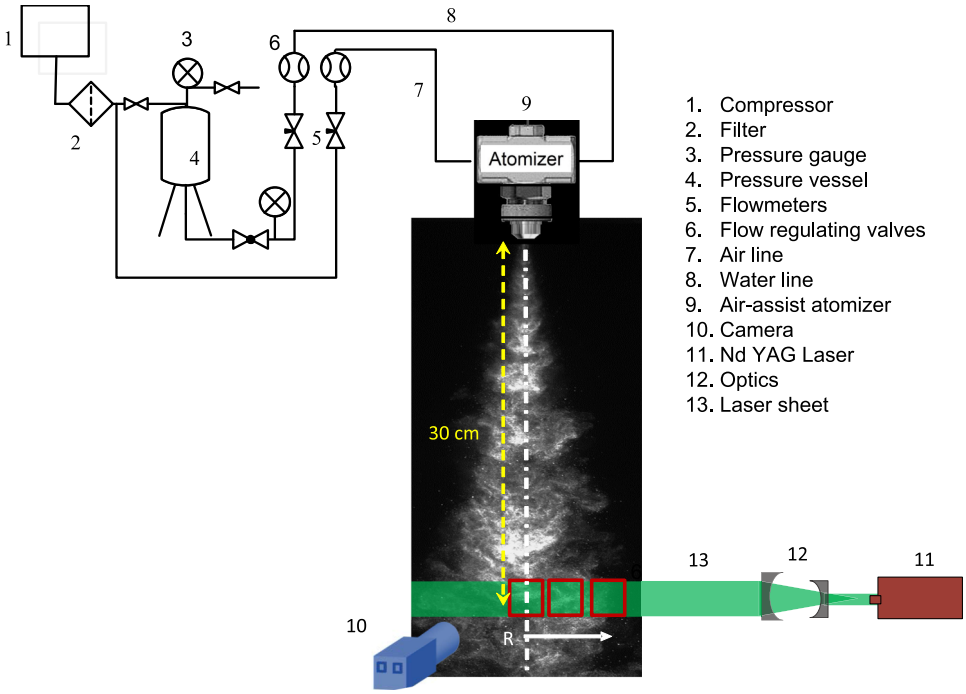

FIG. 1. Schematic of the experimental setup.

droplet and gas velocity, and ρ_l and ρ_a are the liquid and air density, respectively. The measurement of the above statistical quantities will be detailed later. Table I presents the liquid volume loading ratio and mass fraction at the measurement location at the spray center for different injector operating conditions. It can be observed that ϕ_m varies in the range 0.01–0.07 and is higher when either Q_l or Q_a is increased (while the other is held constant), although the effect of increasing the air flow rate is greater due to better atomization in such a case. As explained in Manish and Sahu (2019), considering that $\overline{U} \approx \overline{U_g}$ in the present case (as will be shown later), $\phi_m \approx \alpha/(\alpha + \rho_g/\rho_l)$. Thus, ϕ_m is proportional to α. In the current experiments, for the higher air flow rate (at the same liquid flow rate into the injector), α (and so does ϕ_m) increases nearly four times (Table I) due to better atomization. Although droplet size reduces (though not significantly, as will be shown later) in such a case, the droplet number density increases by nearly four times.

From here onwards, the four operating flow conditions will be denoted by the corresponding liquid mass fractions estimated at the measurement location at the spray center (the last column in Table I). An alternate option is to consider the global liquid mass loading ratio, $\phi_{global} = \rho_l Q_l/(\rho_l Q_l + \rho_a Q_a)$, which is calculated based on the inlet fluid flow rates to the injector. Unlike ϕ_m, this quantity is obviously independent of the droplet measurement method. However, due to air entrainment into the spray, $\phi_m \ll \phi_{global}$ and ϕ_{global} does not represent the local liquid loading, whose effect on droplet clustering is one of the objectives in the present investigation. Hence, ϕ_m was used instead of ϕ_{global} to represent different injector operating conditions. In the current experiments, $\alpha < 0.003$; hence, droplet-droplet interactions leading to droplet collision and coalescence are negligible (Hardalupas *et al.*, 1989 and Finotello *et al.*, 2017). Although, since $\alpha > 10^{-5}$, "two-way coupling" between the dispersed and the carrier phases is possible (Elghobashi, 1994).

TABLE I. Operating flow conditions of the injector and the average liquid volume loading ratio (α) and mass fraction (ϕ_m) at the central measurement station 30 cm downstream of the injector exit.

Inlet water flow rate, Q_l (LPM)	Inlet air flow rate, Q_a (LPM)	Estimated at $R = 0$ mm and $Z = 30$ cm	
		α	ϕ_m
0.025	15	1.5×10^{-5}	0.01
0.050	15	2.0×10^{-5}	0.02
0.025	25	6.4×10^{-5}	0.05
0.050	25	8.9×10^{-5}	0.07

The measurement of droplet clusters using Voronoi diagrams demands identification of individual droplets. This was achieved by planar laser sheet imaging of the spray droplets. A dual pulse Nd:YAG laser (Quantel, EverGreen: 145 mJ/pulse at 532 nm; 5 mm beam diameter) was used to illuminate the spray. For this purpose, the laser beam was converted to a sheet (height and thickness about 5 cm and 1 mm, respectively) using suitable optics. The scattered light from droplets was collected through a lens (50 mm; f/1.8D Nikon lens) and a suitable bandpass optical filter. The focused droplet images were captured using a CCD camera (PCO Pixelfly: 14 bit, 1040×1392 pixels^2) placed at an angle of 90° with respect to the plane of the laser sheet. The field of view was about 1.3 cm × 1.6 cm such that the spatial resolution was about 12 μm/pixel. A small field of view is selected such that the spatial resolution is high enough to capture individual droplets. Although droplets with size below 12 μm were present in the measured droplet size spectrum (as shown later), identifying those droplets was still possible thanks to diffraction limited imaging in the current optical setting of the camera.

However, the dimensions of the measurement area were comparable to the spray half-width, which was about 2.0 cm. The droplet number density was measured by counting the number of identified droplets in the captured images, which corresponds to a measurement volume defined by the image area and the thickness of the laser sheet. The droplet velocity was measured by the Particle Image Velocimetry (PIV) technique by capturing double frame images corresponding to dual pulses of the laser followed by intensity based cross correlation of the image pair. The interrogation window size was about 100 pixels such that the window contains enough droplets, which ensures high correlation in PIV image processing. Thus, the first frame of each PIV image pair was used for Voronoi analysis and measurement of droplet number density, while both frames were used for determining droplet velocity. Measurements were obtained for three different radial measurement stations at R = 0 mm, 20 mm, and 30 mm from the injector axis, where R represents the radial location of the center of the measurement area at each station (Fig. 1). The injector was mounted on an aluminum frame and was traversed for measurements at different radial locations (measurement stations) within the spray. The laser repetition rate was set to 5 Hz such that the acquired images were statistically uncorrelated.

In the present experiments, the droplet size was measured using the Interferometric Laser Imaging for Droplet Sizing (ILIDS) technique. ILIDS is a planar defocusing technique based on identifying the interference pattern, due to the reflected and the first order refracted light scattered from a droplet, on a defocused plane (Glover *et al.*, 1995; Damaschke *et al.*, 2005; and Tropea, 2011). Introduction of a pair of cylindrical lenses between the objective and the CCD camera leads to optical compression of the circular fringe pattern for each droplet in the vertical direction only such that each droplet is imaged as a rectangular region with a superimposed fringe pattern (Maeda *et al.*, 2002). This way, relatively droplet dense regions can be probed. The number of fringes present in each of the recorded interference fringe patterns is proportional to the droplet diameter. The velocity of individual droplets can be obtained in the ILIDS technique by capturing image pairs using both laser pulses similar to PIV. The details of the algorithm for ILIDS image processing used in the present work can be found in Hardalupas *et al.* (2010) and Sahu (2011). It should be mentioned here that the validation ratio in the ILIDS technique, i.e., the ratio of the number of validated to identified droplets, is about 30%, while not all droplets which appear in an image are identified. This is due to various image processing criteria which are imposed while measuring droplet size and velocity from droplet fringe patterns. The droplet rejection rate is high especially in the present case where the droplet loading is on the higher side. We find typically 10–20 validated droplets in each ILIDS image. It is important to note that in contrast to PIV, which measures velocity of groups of droplets, in ILIDS, the velocity of individual droplets is measured, although the spatial resolution in the latter is poor due to less number of validated droplets. However, we again mention here that in the present work, the droplet clusters were characterized using Voronoi analysis on the droplets identified on the PIV images in which case the number of identified droplets is much higher than that in the ILIDS images. The ILIDS technique was used only for statistical characterization of size and velocity of the spray droplets.

For each flow condition and measurement station, 1000 PIV image pairs were captured for Voronoi analysis and measurement of droplet velocity and number density, while 1500 images were collected for droplet sizing by the ILIDS technique. The number of images captured for each technique was such that statistical convergence of all droplet statistics was always ensured. The processing of PIV and ILIDS images was carried out using in-house codes based on MATLAB. The application of the above techniques can provide an instantaneous spatial map of droplet velocity and also gas velocity (by assuming small droplets in the ILIDS images to follow the gas phase as will be explained later). However, in the present experiments, due to inadequate spatial resolution in both techniques, the droplet and gas velocity vector plots are not useful to gain physical insight into the droplet clustering process and also to characterize the clusters. In fact, this further emphasizes the advantage of the Voronoi analysis to study droplet clustering in the spray. Nevertheless, the droplet and gas velocity statistics obtained from the two techniques are helpful to explain the physics behind the observations through the Voronoi analysis.

B. Characterization of droplet clusters

In the literature, a broad range of methods have been described for statistical characterization of particle clusters. These methods include calculation of the *clustering Index* (Shaw *et al.*, 2002), *pair correlation function* also known as *radial distribution function* or RDF (Saw *et al.*, 2008 and Sundaram and Collins, 1999), *Minkowski functions* (Calzavarini *et al.*, 2008), *box counting method* (Aliseda *et al.*, 2002; Fessler *et al.*, 1994; and Scott *et al.*, 2009), *Voronoi analysis* (Monchaux *et al.*, 2010 and Sumbekova *et al.*, 2017), etc. Recently, Monchaux *et al.* (2012) reviewed the above methods and summarized the advantages and limitations of each approach. We have reported statistical measurement of droplet clusters under current operating flow conditions based on the measurement of the D parameter (which quantifies degree of clustering) using the box counting approach in a recent article (Manish and Sahu, 2019). There the focus was on investigating any link between the measured turbulent droplet number flux and cluster statistics. However, that approach is not suitable for identifying individual clusters, which is the basis of the present work. In the present paper, droplet clustering in sprays is studied using Voronoi diagrams, which has some distinct advantages in comparison to the other approaches as outlined in the following: (a) instantaneous particle clusters are identified using the Voronoi diagrams such that the local particle concentration maps can be obtained and, in addition, geometric characterization of individual particle clusters is possible, while the other approaches such as RDF or cell counting can only provide cluster statistics; (b) there is no necessity to prescribe a length scale to quantify the degree of clustering as for the methods like clustering index or cell counting method; (c) it is found to be computationally less time consuming in comparison to other methods such as RDF; and (d) finally, calculation

of Voronoi diagrams allows characterization of "voids" in addition to "clusters." The importance of the study of voids will be explained later. The unique capability of Voronoi analysis for visualization and characterization of particle clusters as well as voids makes it a suitable tool to gain deep insight into the dynamics of droplet clustering and this justifies the rationale behind the usage of Voronoi analysis in the present work.

1. Voronoi analysis of droplet clusters

A Voronoi diagram, also known as Dirichlet decomposition, is a tessellation where a tile corresponding to a given data point is a locus of all points of space closest to this data point (Andronov *et al.*, 2016). There are various fields where Voronoi diagrams find applications ranging between biological studies, astronomical studies, medical diagnosis, and so on. The usefulness of Voronoi diagrams for studying preferential accumulation of particles/droplets in two-phase flows was first demonstrated by Monchaux *et al.* (2010) and has been reported by several authors thereafter (Monchaux, 2012; Obligado *et al.*, 2011; Sumbekova *et al.*, 2017; Charalampous and Hardalupas, 2011; and Lian, 2014 to name few). For the current injector operating conditions, the potential of Voronoi analysis for studying clustering of spray droplets has been demonstrated in Manish and Sahu (2018).

The flowchart for identifying individual droplet clusters in an instantaneous PIV image based on calculation of the Voronoi areas is depicted in Fig. 2. The first step in this process is to identify droplet centres in the instantaneous spray image. This is achieved by binarization of the image using optimum intensity thresholding based on Otsu's algorithm followed by identification of centroids of the droplets. In the next step, the Voronoi cells (which are essentially polygons) around the centre of each droplet are obtained using the inbuilt MATLAB function. The areas of all Voronoi cells are calculated. For randomly distributed droplets, the distribution function for the normalized Voronoi areas can be represented by the Random Poisson Process (RPP), as described in the following equation

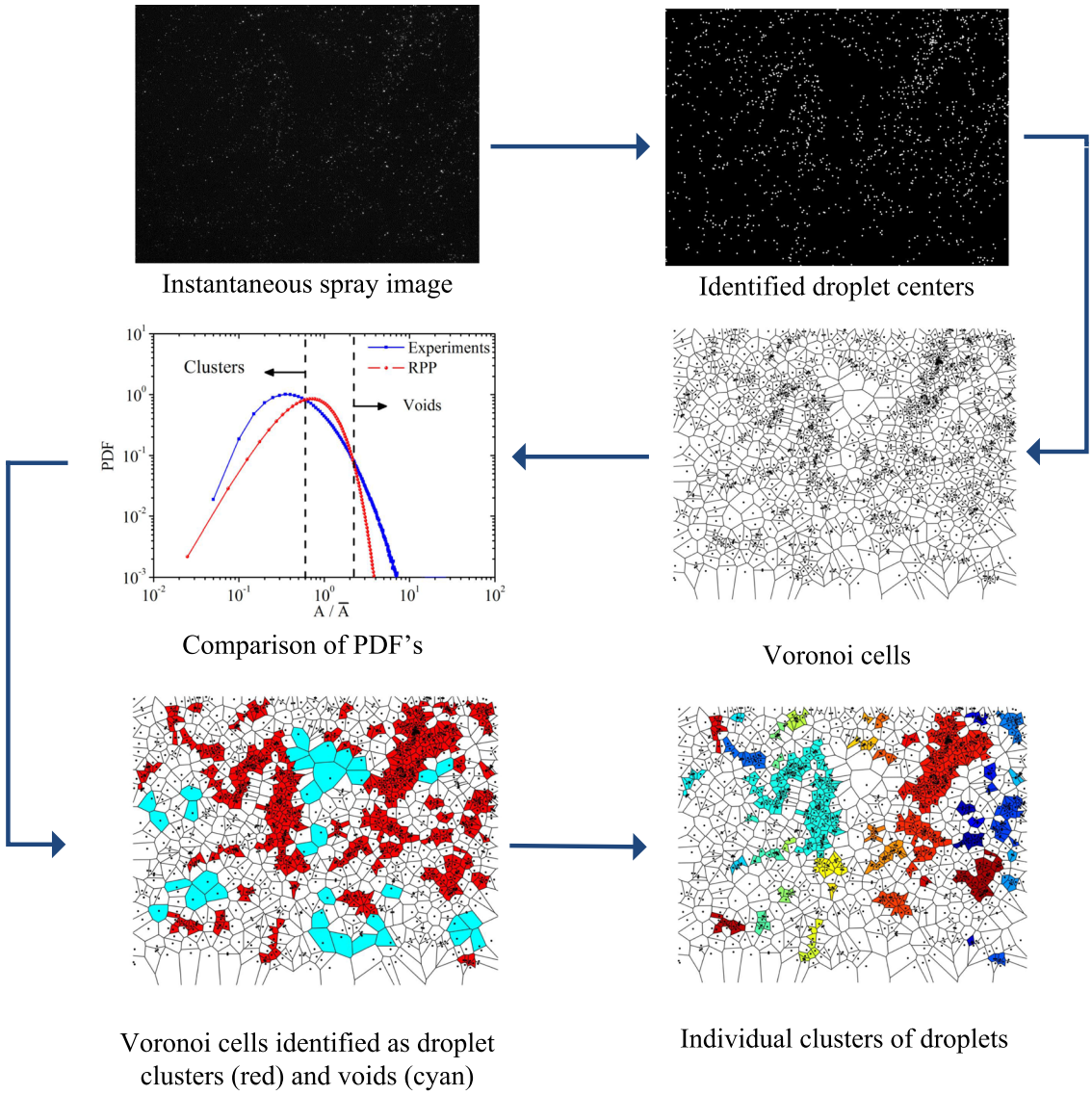

FIG. 2. Flow chart to identify droplet clusters and void areas using Voronoi diagrams. The final plot indicates individual droplet clusters shown in different colors.

(Ferenc and Néda, 2007):

$$f_{2D}(y) = \frac{343}{15}\sqrt{\frac{7}{2\pi}}y^{5/2}\exp^{-7y/2}. \quad (2)$$

The probability distribution function (PDF) of the normalized Voronoi areas (Voronoi area, A, normalized with the average area, $\overline{A}$, i.e., $A/\overline{A}$) obtained from the experiment is compared with that for the RPP distribution [Eq. (2)] and the intersection points of both PDFs are found out. Usually, the two PDFs intersect twice (see Fig. 2). The Voronoi cells whose areas are smaller than the first intersection point are considered to belong to a droplet cluster, whereas the Voronoi cells whose areas are larger than the second intersection point are considered as voids (Monchaux *et al.*, 2010). The next step is to recognize individual droplet clusters among all Voronoi cells identified as droplet clusters. For this purpose, the cells which share at least one common side are identified and such interconnected cells are accepted as individual clusters of droplets (Fig. 2). The individual void areas were also obtained in a similar way. Figure 3 shows examples of the application of the Voronoi analysis for different local liquid mass fractions (ϕ_m) at the central spray measurement location ($R = 0$ mm). We note that the intersection points of the PDFs (which set the limits to categorize a Voronoi cell as either a cluster or void) vary with each measurement, i.e., depending on the injector operating conditions and also radial measurement stations. Also, since these cutoffs are statistically obtained considering the image ensemble, it is possible that even if the droplets appear to be closer, their corresponding Voronoi areas are larger than the chosen cutoff and hence remain unidentified as clusters. However, we could find only few such instances (one in 20 images) in our experiments. As mentioned earlier, the size of Voronoi cells is inversely related to local droplet concentration. Thus, the middle column in Fig. 3 essentially depicts the topology of the high droplet concentration regions in the plane of measurement, while the last column in the same figure shows the void areas that denote the regions of very low droplet concentration. Hence, the void areas are larger than that of the clusters. Note that such measurements are unique to Voronoi area calculation. One important observation is that droplet clustering occurs over a broad range of length scales, i.e., clusters as well as voids of different sizes are evident for all cases.

As suggested by Monchaux *et al.* (2010), the degree of clustering can be quantified by calculating and comparing the standard deviations of the measured Voronoi areas (σ_v) and that for droplets distributed as per RPP (σ_{RPP}). The standard deviation of the 2D RPP distribution [Eq. (2)] is equal to

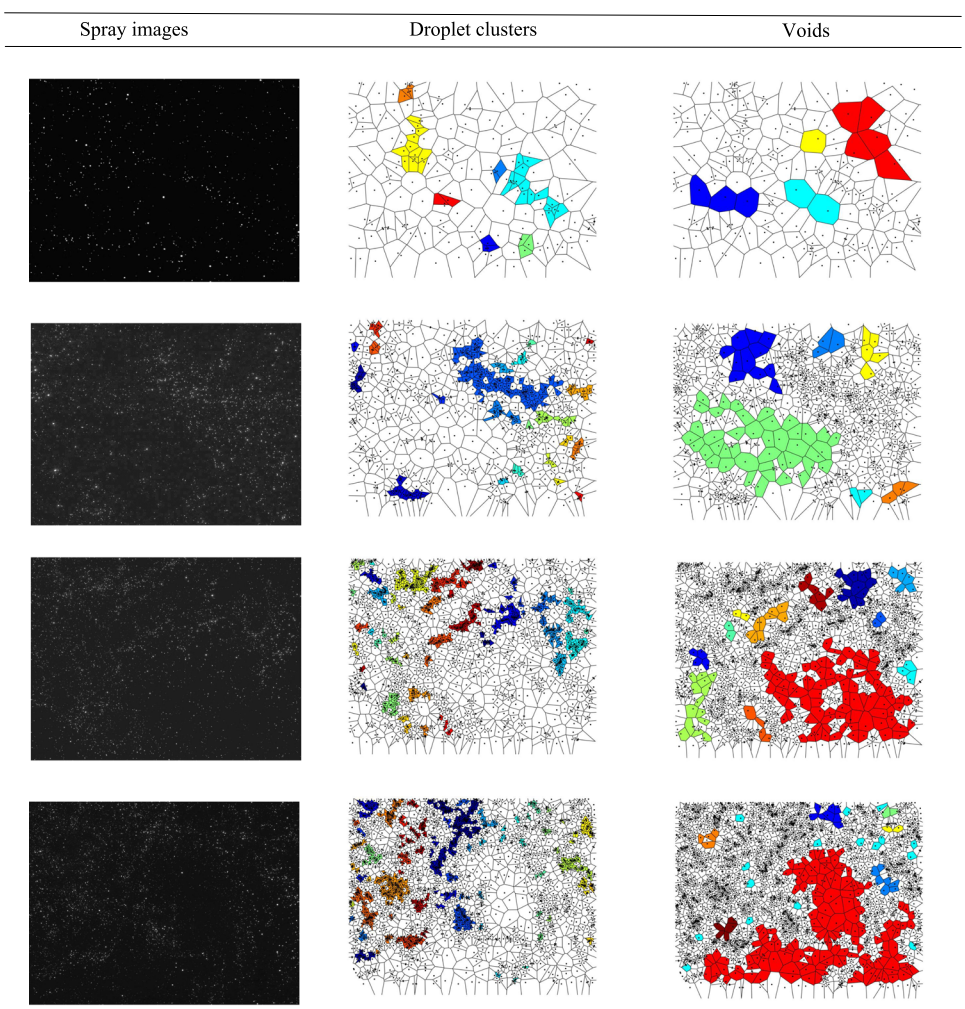

FIG. 3. Examples of application of Voronoi analysis of the spray images for different local liquid mass fractions at the measurement location at $R = 0$ mm. Left column: instantaneous spray image, middle column: identified individual droplet clusters (shown in different colors), and right column: individual voids (shown in different colors).

0.53 (Ferenc and Néda, 2007). When droplets preferentially accumulate in some region of the flow, their distribution is non-random and the corresponding standard deviation of the Voronoi areas is greater than that for the RPP distribution. Thus, a parameter σ_{rel} can be defined as per the following equation, which is an indicator of the degree of droplet clustering:

$$\sigma_{rel} = \frac{\sigma_v - \sigma_{RPP}}{\sigma_{RPP}}. \tag{3}$$

Thus, the condition $\sigma_{rel} > 0$ implies non-random distribution of droplets, and higher values of σ_{rel} means stronger droplet clustering.

2. Biases in Voronoi calculation

The calculation of Voronoi areas is subjected to inherent biases mainly due to two reasons: (a) two-dimensional (2D) imaging of the droplets and (b) sub-sampling as a consequence of intensity thresholding for identifying droplets (Monchaux, 2012). The former refers to the bias due to the projection of the three-dimensional positions of the droplets on the plane of imaging. However, in their numerical analysis based on the Direct Numerical Simulation (DNS) of particle-laden flow, Monchaux (2012) found very good quantitative agreement between the 2D and 3D calculations of σ_{rel}, which suggests reliability of using the 2D imaging for Voronoi calculation. The second reason for the bias is related to the intensity of scattered light from the droplets. Due to the Gaussian distribution of light intensity across the laser sheet (in a direction perpendicular to the plane of the laser sheet), the scattering intensity of a droplet depends on its location within the laser sheet and also on the droplet size. As a consequence, intensity thresholding to identify the droplets may result in significant underestimation (more than 50%) of particle concentration (Knowles and Kiger, 2012). Similarly, the inhomogeneous illumination in the vertical direction due to the Gaussian profile of the laser beam can lead to detection of more particles in the region corresponding to higher light intensity (Sumbekova *et al.*, 2017). This can lead to bias in the analysis of the clustering properties of the particles, without an appropriate calibration. However, in our experiments, the height of the laser sheet (about 5 cm) was larger than that of the imaging area (which was about 1.2 cm) such that no strong gradients in the light scattering intensity in vertical direction were present. Thus, any possible bias due to light intensity variation in the vertical direction on clustering statistics is expected to be minimal.

In order to examine the effect of thresholding on the calculation of the distribution of Voronoi areas in the present case, the threshold value (obtained from Otsu's algorithm as mentioned earlier) was moderately varied by ±20%, which was found to result in about ±20% variation in the total droplet number count. Figure 4(a) shows the normalized PDF of Voronoi areas for different threshold values equal to β (=0.8 –1.2) times the original threshold for the case $\phi_m = 0.01$ and $R = 0$ mm, as an example. It is observed that the PDF does not change much with the intensity thresholding although some differences are noticed for very small cells. Similar results were obtained for other injector operating conditions as well. The dependence of σ_v (which signifies the degree of droplet clustering) on intensity thresholding is presented in Fig. 4(b) for different local liquid mass fractions at the central measurement location at $R = 0$ mm. While for $\phi_m = 0.01$, there is negligible variation of σ_v with respect to β, a slight reduction is observed for higher ϕ_m. However, considering the uncertainty in σ_v (about ±5%), it can be concluded that the calculation of σ_v is nearly independent of intensity thresholding in the present experiments. Our results are in good agreement with those of Monchaux (2012), who demonstrated the robustness of application of Voronoi analysis for processing of 2D experimental images to study preferential particle accumulation. Note that in Fig. 4(b), σ_v increases with local liquid mass fraction indicating a greater degree of droplet clustering. This will be discussed again later.

3. Geometric characterization of droplet clusters

Once individual droplet clusters are identified following the method described earlier, the area and perimeter of each droplet cluster (denoted as A_c and P_c) are calculated using inbuilt MatLab functions (Monchaux *et al.*, 2010; 2012). The length scale of the droplet clusters (L_c) is also of interest since its comparison with turbulent eddy length scales can elucidate on the influence of eddies of different sizes on droplet dispersion and clustering. While the earlier studies (Lian, 2014; Monchaux *et al.*, 2010; Sumbekova *et al.*, 2017; and Rabencov and van Hout, 2015) estimated the cluster length scale as the square root of cluster area, i.e., ($\sqrt{A_c}$), this approach does not always hold good for droplet clusters, especially, of

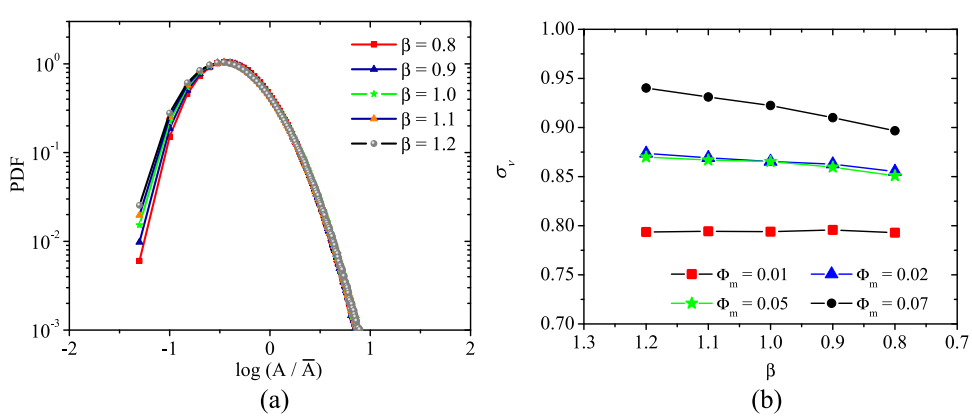

FIG. 4. Sensitivity analysis in Voronoi area calculation: (a) PDF of the normalized Voronoi areas for different intensity threshold values for $\phi_m = 0.01$ at $R = 0$ mm. (b) Dependence of σ_v on intensity thresholding for different liquid mass fractions at $R = 0$ mm.

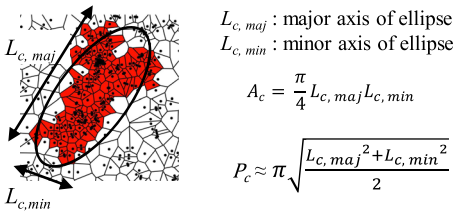

FIG. 5. Geometric characterization of droplet clusters. A_c and P_c are the area and perimeter of a cluster obtained from Voronoi area calculation.

larger areas. For long slender clusters (see Fig. 5 as an example), the above method leads to a length scale which is always closer to the smaller dimension of the cluster, i.e., the cluster thickness, thereby underestimating the actual length scale of the clusters. Hence, an alternate approach was used in the present work, where the major and minor axes of an ellipse of the same area and perimeter as those of a droplet cluster were determined. These two length scales are denoted as $L_{c,maj}$ and $L_{c,min}$ corresponding to the major axis and the minor axis of the ellipse, respectively. A quadratic expression for either $L_{c,maj}$ or $L_{c,min}$ is obtained from the perimeter and area of each cluster which gives two roots for each axis. The real roots are finally considered. Figure 6(a) shows a scatter plot of the ratio of $L_{c,maj}$ to $L_{c,min}$ versus normalized cluster area ($A_c/\overline{A_c}$) for $\phi_m = 0.01$ at $R = 0$ mm as an example. A similar plot is shown for the ratio of conventionally measured length scale, $L_{c,conv}$ ($=\sqrt{A_c}$) and $L_{c,min}$ in Fig. 6(b), which is much less scattered and indicates that the two length scales are always close to each other which confirms our earlier argument. It is interesting to observe that as anticipated earlier, only for clusters with smaller areas, the ratio $L_{c,maj}/L_{c,min}$ is close to $L_{c,conv}/L_{c,min}$. However, for clusters of larger areas, $L_{c,maj}$ can be even up to 6 times $L_{c,min}$. This means that for such cases, the droplet clusters are elongated in some direction such that determining an equivalent diameter based on ($\sqrt{A_c}$) would lead to significant bias in the measurement of length scale of droplet clusters. Finally, the length $L_{c,maj}$ is considered as a representative length scale of droplet clusters. Further results on comparison of length scales of droplet clusters for different liquid mass fractions as well as measurement locations appear in Sec. III. The length scale of individual void areas (both $L_{v,conv}$ and $L_{v,maj}$) was also calculated following the same approach as detailed above for droplet clusters.

III. RESULTS AND DISCUSSION

A. Characterization of droplets and air flow turbulence

The probability of droplet size distributions measured by the ILIDS technique is shown in Fig. 7 for different radial measurement stations. For each location, the results are shown for different local liquid mass fractions. The Arithmetic Mean Diameter (AMD) and Sauter Mean Diameter (SMD) were calculated and are shown in Table II for $R = 0$ mm. In general, the AMD and SMD were found to be about 15 μm and 30 μm, respectively, and do not vary much across the spray, which is expected since the measurement locations are situated far downstream of the nozzle exit. However, the average droplet size was always smaller when the gas flow rate at the injector inlet is made higher at the same water flow rate (compare columns for $\phi_m = 0.01$ and 0.05, and $\phi_m = 0.02$ and 0.07 in Table II). The scatter plot of droplet size and velocity is shown in Fig. 7(d) for $\phi_m = 0.07$ and $R = 0$ mm location as an example. Similar results were obtained for other measurement locations and injector operating conditions. It can be observed that the droplet velocity does not bear a strong correlation with droplet size. This is due to the choice of the axial measurement location far downstream of the injector exit where the initial jet momentum due to the jet breakup process (at the injector exit) has been dissipated. The droplet dynamics at such locations is mostly governed by the entrained air flow since the droplet-gas slip velocity significantly reduces away from the injector exit (Gounder *et al.*, 2012). This is further supported by the estimated Stokes number of droplets based on large scale eddies, which was found to be far below 1 (as will be shown later).

Though not shown here, the average droplet number density ($\overline{N}$) was higher for higher ϕ_m for all radial measurement stations. The trends for the droplet velocity (measured by the PIV technique) and its radial variation across the spray were similar to those for a single phase turbulent jet. The axial component of the mean droplet velocity was maximum at the spray center and reduced towards the spray boundary, while the mean radial velocity was negligibly small for all radial locations. The radial location where the mean axial velocity was 50% of its value at the spray center was defined as the half-width of the spray ($R_{1/2}$). The jet spread rate ($=R_{1/2}/Z$) was about 0.065–0.081 (smaller for higher ϕ_m) and lower than that for

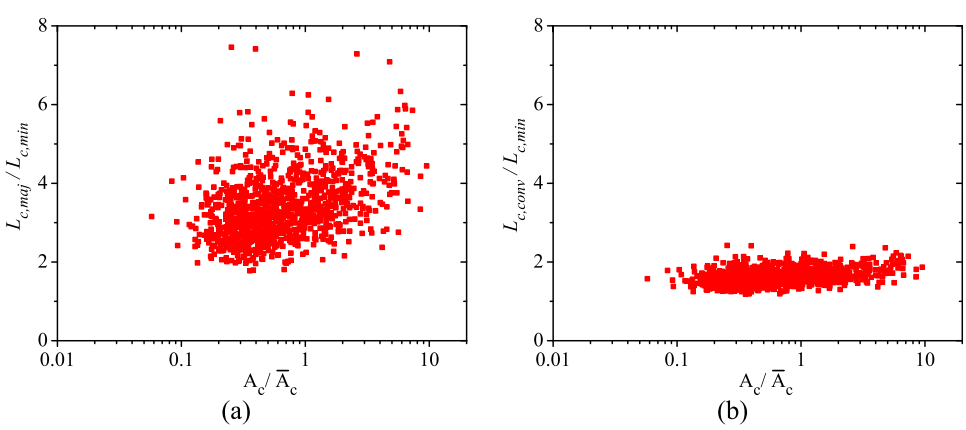

FIG. 6. Scatter plots of (a) $L_{c,maj}/L_{c,min}$ and (b) $L_{c,conv}/L_{c,min}$ versus normalized cluster area ($A/\overline{A_c}$) for the injector operating condition $\phi_m = 0.01$ at $R = 0$ mm.

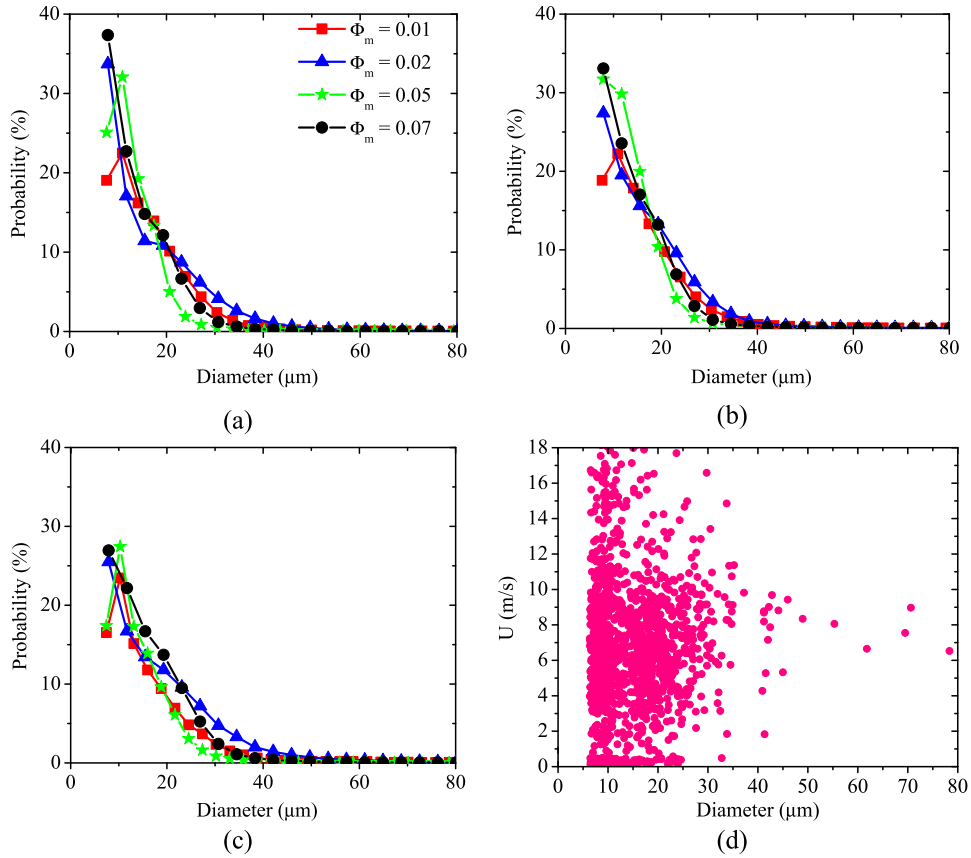

FIG. 7. Droplet measurement by the ILIDS technique. Probability of droplet size distribution at the radial measurement stations R = (a) 0 mm, (b) 20 mm, and (c) 30 mm. (d) Scatter plot of droplet size and velocity measured by the ILIDS technique for $\phi_m = 0.07$ at $R = 0$ mm.

a single phase turbulent jet for which the spread rate is about 0.1 (Pope, 2001). Since for a single phase turbulent jet the entrainment rate and the decay rate are proportional to the jet spread rate (Pope, 2001), the differences in the spread rate of the spray jet for various injector operating conditions highlight the differences in the entrainment dynamics.

The droplet Stokes number, St ($=\tau_d/\tau_f$), was evaluated based on the droplet response time ($\tau_d = \rho_l D^2/18\mu$, where ρ_l and μ are the liquid density and gas viscosity, respectively), and the characteristic time scale of the gas flow surrounding the droplets, τ_f [$= R_{1/2}/u_{gr}$, where u_{gr} is the root mean square (rms) of fluctuations of the gas flow] was also evaluated. We note that based on the measurement of velocity of individual droplets by the ILIDS technique, the droplets with size below 15 μm were assumed to be air flow tracers since the corresponding Stokes number was found to be very small (<0.05). The droplet velocity statistics measured by ILIDS was about 1–1.5 times that by PIV, and the difference was higher for lower droplet mass loading. As explained earlier, the reason behind this is due to measurement of individual velocity in the former technique in comparison to that of a group of droplets in the latter. In the present case, the ILIDS data were used to estimate different statistical quantities (see Table II) for characterization of droplet and gas phase turbulence as detailed

TABLE II. Droplet and air turbulence characteristics at the central measurement station at $R = 0$ mm and $Z = 30$ cm for different injector operating conditions.

Liquid mass fraction, ϕ_m	0.01	0.02	0.05	0.07
Mean axial droplet velocity, $\overline{U}$ (m/s)	6.3	6.4	6.5	7.1
Droplet axial velocity fluctuations, u_r (m/s)	1.7	1.8	2.4	2.7
Mean gas phase (tracer droplets) axial velocity, $\overline{U}_g$ (m/s)	6.5	6.6	7.0	7.3
Gas phase (tracer droplets) axial velocity fluctuations, u_{gr} (m/s)	2.1	2.2	2.8	2.9
Half width of the spray, $R_{1/2}$ (mm)	24.5	22	22	19.5
AMD at $R = 0$ mm (in μm)	17	17	14	15
SMD at $R = 0$ mm (in μm)	28	32	26	29
St based on AMD	0.08	0.09	0.07	0.10
St based on SMD	0.21	0.32	0.26	0.39
Gas phase turbulent Reynolds number, Re_g	7445	8420	9782	10098
Kolmogorov length scale, η (in μm)	52	46	39	37
St_η based on AMD	4.3	6.2	5.2	6.6
St_η based on SMD	13.0	19.3	18.3	25.5

below. As shown in Table II, the root mean square (rms) of droplet axial velocity fluctuations (u_r) is about 20%–40% of the mean droplet velocity ($\overline{U}$). The rms of radial velocity fluctuations (v_r) was also calculated and the ratio u_r/v_r was found to be in the range 1.4–1.6 indicating that the air flow turbulence is anisotropic, again similar to a turbulent jet. It can be observed in Table II that the mean and fluctuations of tracer droplet (gas) velocity ($\overline{U_g}$ and u_{gr}) are close to those of droplet velocity further highlighting the weak droplet size-velocity correlation presented in Fig. 7(d).

Thus, the characteristic time scale of the gas flow is obtained based on the velocity of these tracer droplets and the spray half-width. Finally, the droplet Stokes number based on AMD was about 0.1 and that based on SMD was about 0.2–0.4 (Table II). This suggests that the droplets partially respond to the large scale eddies of the air flow turbulence. Hence, it is possible that the droplets preferentially accumulate in some region of the flow leading to clusters of droplets. The local turbulent Reynolds number ($Re_g = u_{gr}R_{1/2}/\nu$) of the gas phase is one of the important parameters that influences preferential accumulation of droplets. In the present case, Re_g was calculated based on $R_{1/2}$ and axial velocity fluctuations of tracer droplets and found to be in the range 7000–10 000. It is noted here that the air flow turbulence characteristics vary across the spray. Thus, the droplet Stokes number is smaller from $R = 0$ mm to $R = 30$ mm implying better response of droplets to gas flow near the spray boundary. Since the calculated Weber number (We) of droplets in the present experiments was about 0.02, which is far below the critical value ($\approx$10), no secondary breakup of droplets is expected and hence the measured droplet size distribution is stable. Since the terminal velocity ($=\tau_d \times$ g) was much smaller than the fluctuations of droplet axial velocity, the influence of gravity on droplet motion can be neglected (Attari *et al.*, 2016). Also, evaporation of water droplets was not important in the present case since the time scale of droplet evaporation ($\approx$120 ms) was much larger than the residence time of droplets ($\approx$3.45 ms) within the measurement area.

We note that in the present experiments, it is not possible to obtain spatially resolved gas velocity measurement up to the smallest scale of turbulence especially due to high droplet mass loading. For such cases, the existing phase-separation approaches, while using the PIV technique, have limitations to provide reliable measurements (Sahu *et al.*, 2018b). Nevertheless, considering that strong influence of small scales of turbulence on droplet clustering has often been reported in the literature on preferential accumulation of particles (as cited earlier), we obtained a rough estimate of the Kolmogorov scales based on the scaling laws (Tennekes and Lumley, 1972). The Kolmogorov length and time scales (η and τ_η) were calculated via the estimation of the dissipation rate ($\sim u^3_{gr,D<15\mu}/R_{1/2}$). As shown in Table II, η is about 30–50 μm (note that η is consistently smaller for higher Re_g, which is expected and gives some confidence on the rough estimates). The Stokes number based on the smallest scale St_η is about 5 and 20 when calculated considering AMD and SMD of droplets, respectively, which suggests poor response of droplets to the smallest turbulent eddy. Finally, this highlights a wide range of droplet responses to turbulent eddies within the spray ($St \sim 0.05$–20) for all experiments. Also, notice that the droplet size is not negligible and is rather comparable to η.

It is worth mentioning here that the structure of a spray and the associated flow field are sensitive to the nozzle design. Since we have not characterized sprays from different nozzles, it may not be possible to generalize the present results for other injectors. Nevertheless, some general inference on droplet clustering can be gained based on our results because (i) in the present work, the droplet measurements were obtained far downstream from the injector exit such that the memory of the primary liquid breakup process close to the injector exit is expected to be forgotten. The droplet dynamics at such location is governed mainly by the entrained air flow turbulence. Hence, our results can be compared to other injectors as long as the region of interest is far downstream and the Stokes number of droplets based on large scale eddies is much below "one," as in the current experiments. (ii) Most of the results pertaining to droplet clustering were discussed essentially in terms of non-dimensional numbers, i.e., St, ϕ_m, and Re_g. Thus for the same range of the above non-dimensional numbers, at least the gross features of droplet clustering, for instance, multiscale clustering of droplets and strong dependency of cluster statistics on liquid mass loading (as will be explained later), can be expected. However, in sprays, the above three parameters are not independent of each other and this can be injector specific.

B. Influence of local liquid mass loading on droplet clustering

1. Distribution of areas of droplet clusters and voids

Figure 8(a) presents the probability of areas of droplet clusters (A_c) for different local liquid mass fractions (ϕ_m) at $R = 0$ mm. Notice that the area of droplet clusters spans over a wide range from about 0.1 mm^2 to about 10 mm^2 for all cases. This suggests that droplet clustering in sprays is a multiscale phenomenon and occurs due to droplet dispersion by turbulent eddies of various sizes. It can be also observed in Fig. 8(a) that each PDF exhibits a distinct peak (that indicates the existence of a typical characteristic cluster dimension) after which there is an algebraic decay. It is interesting to notice in Fig. 8(a) that the peak in the PDFs shifts towards left for higher ϕ_m for which the corresponding average cluster area ($\overline{A_c}$) was also found to be smaller. This implies generation of smaller clusters as the local liquid mass fraction is higher for which the degree of clustering was also higher as was shown in Fig. 4(b). It may appear obvious that the average cluster size is smaller for higher ϕ_m, which corresponds to a larger average number count of droplets in the same measurement area and hence smaller areas of Voronoi cells. However, we note that, as explained earlier, the classification of a Voronoi cell as a part of a cluster is decided based on comparison of normalized cluster areas ($A_c/\overline{A_c}$) with a RPP distribution based on the same average number of droplets. Thus, had the droplets been randomly distributed, identifying clusters would not have been possible even if the droplet loading is higher. In other words, the results obtained above are a consequence of interaction of droplets due to air flow turbulence rather than simply due to increase/decrease in the droplet count in the

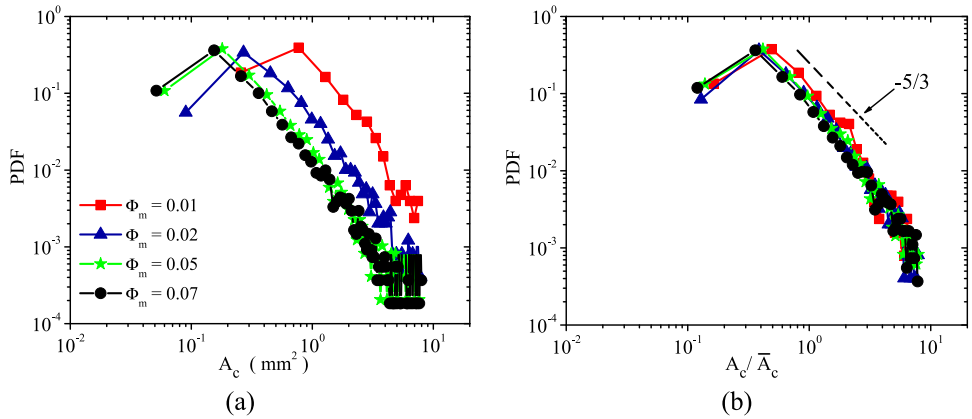

FIG. 8. PDF of (a) cluster area A_c and (b) normalized cluster area $A_c/\overline{A_c}$ for different liquid mass fractions at $R = 0$ mm.

PIV images. Furthermore, we note that clustering of droplets depends on not only ϕ_m but also Stokes number, St, and gas phase Reynolds number, Re_g (Sumbekova *et al.*, 2017). However, in the present experiments, when ϕ_m increases, the gas phase Re_g is also higher although St did not vary much (Table II). Thus, the increase in the intensity of clustering is attributed to both ϕ_m and Re_g, which, unlike wind tunnel based experiments, cannot be varied independent of each other in the present case.

The PDFs of the normalized cluster area are plotted in Fig. 8(b). The plots for different ϕ_m nearly overlap with each other, and the slope after the peak (i.e., the algebraic decay exponent) is approximately −5/3. This indicates self-similarity of the clustering process. The results for void areas [see Figs. 9(a) and 9(b)] are similar to clusters; i.e., the PDFs shift towards smaller void areas for higher ϕ_m and the exponent for the algebraic decay in the normalized PDFs is −5/3. Nevertheless, for all ϕ_m, the average void areas were always larger than those for droplet clusters ($\overline{A_v} > \overline{A_c}$) and the corresponding distribution is also wider. The self-similar distributions of normalized void areas and the reduction of $\overline{A_v}$ for higher ϕ_m (similar to $R_{1/2}$ and η as shown in Table II) suggest that the voids mimic the turbulent eddies of the air flow around droplets. The above results are similar to those of Sumbekova *et al.* (2017) although in their case the range of A_c was wider. However, in their experiments, both gas phase Reynolds number and length scale of large eddies were larger than those in the present case. However, differences in the results with respect to the above study were observed in the case of measurement of length scale of droplet clusters, which will be explained in Sec. III B 3.

2. Droplet number density within clusters

Having known that the areas of clusters of droplets span over a wide range, the next question that arises is if the droplet concentration within a cluster varies according to its size. For this purpose, the droplet number density within a cluster is calculated as N_c/A_c, where N_c is the number of droplets within a cluster with area A_c. This is normalized with the average droplet number density, $\overline{N}/A$, corresponding to the whole image, where $\overline{N}$ is the average droplet number count over the ensemble of the images and A is the image area. Thus the relative droplet number density [$n_{rel} = (N_c/A_c)/(\overline{N}/A)$] represents the local droplet concentration within droplet clusters relative to the global average value. Figure 10 presents the PDF of n_{rel} for different ϕ_m at the measurement station at $R = 0$ mm. It is observed that n_{rel} is mostly greater than "one" and in the range 1–10. This means that the local concentration of droplets within a cluster can be considerably higher than the global average. A distinct peak is observed for each PDF in Fig. 10, which, surprisingly, does not vary much as the local liquid mass fraction increases.

Figures 11(a) and 11(b) show the scatter plots of n_{rel} versus normalized area of clusters $A_c/\overline{A_c}$ for $\phi_m = 0.01$ and 0.07. Depending on the area of the clusters relative to their average cluster area, basically two distinct trends are observed. For clusters with area $A_c < \overline{A_c}$, an algebraic decay of n_{rel} with

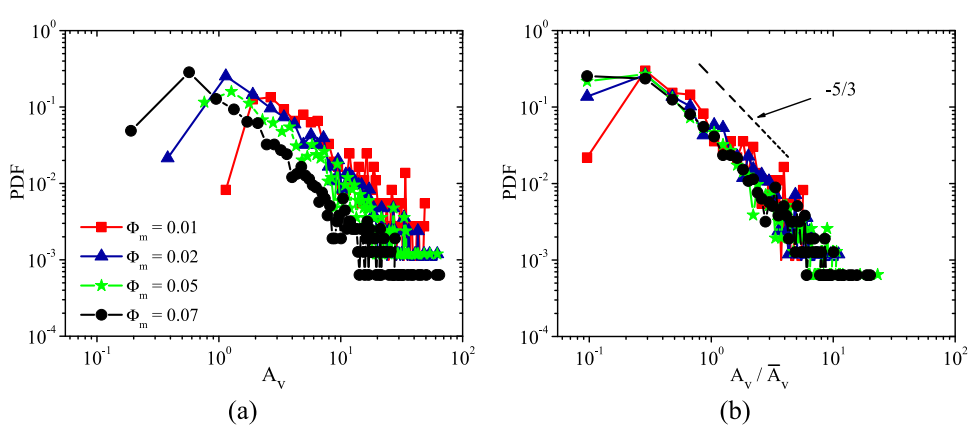

FIG. 9. PDF of (a) void area A_v and (b) normalized void area $A_v/\overline{A_v}$ for different liquid mass fractions at $R = 0$ mm.

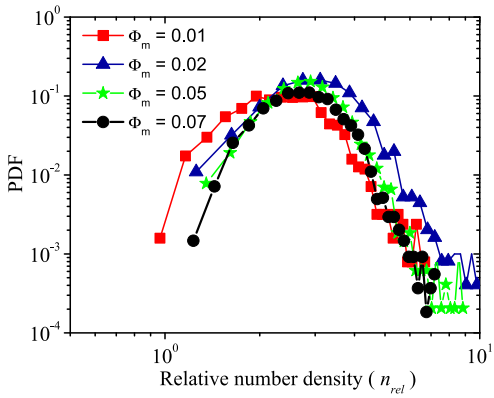

FIG. 10. PDF of the relative droplet number density in droplet clusters (n_{rel}) for different liquid mass fractions at $R = 0$ mm. Reproduced with permission from M. Manish and S. Sahu, "Analysis of droplet clustering in air-assist sprays using Voronoi diagrams," in 14th International Conference on Liquid Atomization and Spray Systems (ICLASS). Copyright 2018 University of Illinois.

respect to area of clusters is evident. However, for $A_c > \overline{A}_c$, n_{rel} is nearly independent of the area of the cluster. No distinct difference in the two plots in Fig. 11 can be observed.

3. Characteristic length scale of droplet clusters

As explained earlier in Sec. II B 1, the characteristic length scale of individual droplet clusters can be obtained from their area and perimeter obtained from the Voronoi diagrams. Two different approaches were outlined. In the first method, the cluster length scale is conventionally calculated as $\sqrt{A_c}$, while in the second method, the major axes of an ellipse ($L_{c,maj}$) of the same area and perimeter as that of a cluster are determined. The PDFs of cluster length scales obtained from both approaches are plotted in Fig. 12(a). The figure presents the results for two different liquid mass fractions, i. e., $\phi_m = 0.01$ and 0.07 at the measurement station $R = 0$ mm. The cluster length scales are normalized with the respective spray half-widths ($R_{1/2}$) as well as Kolmogorov length scale, η. As expected, similar to the distribution of area of the droplet clusters, the corresponding length scales vary over a wide range (nearly an order of magnitude variation can be observed) and the peaks in the PDFs indicate that typical cluster dimensions can be identified. In general, $L_{c,conv} < L_{c,maj}$ and the values approach each other for small clusters ($\ll R_{1/2}$); however, significant difference in the probability of a given cluster size is possible for large clusters (comparable to $R_{1/2}$). As explained earlier in the context of Fig. 6(a), large sized clusters preferentially span along some direction such that their length scale in a perpendicular direction can be much smaller ($L_{c,maj} > L_{c,min}$). This emphasizes anisotropic characteristics of droplet clusters. The droplets, which show good response to the large scale eddies, preferentially accumulate due to such eddies, which are themselves anisotropic in the spray flow. However, for small clusters, $L_{c,maj} \sim L_{c,min}$ implying that they are more isotropic.

The average length scale of clusters ($\overline{L_c}$) and voids ($\overline{L_v}$) was calculated. The statistical uncertainty for both was about ±5% with 95% confidence interval. Since the average cluster and void areas were smaller for higher ϕ_m [Figs. 8(a) and 9(a)], a similar trend is also observed for $\overline{L_c}$ and $\overline{L_v}$ as shown in Fig. 13. These results have the following implications.

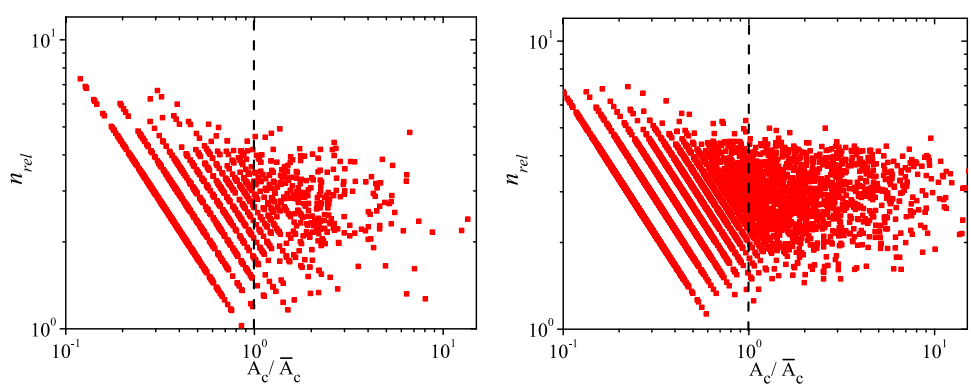

FIG. 11. Scatter plots of relative droplet number density (n_{rel}) and normalized cluster area ($A_c/\overline{A}_c$) for ϕ_m = (a) 0.01 and (b) 0.07 at the measurement station $R = 0$ mm.

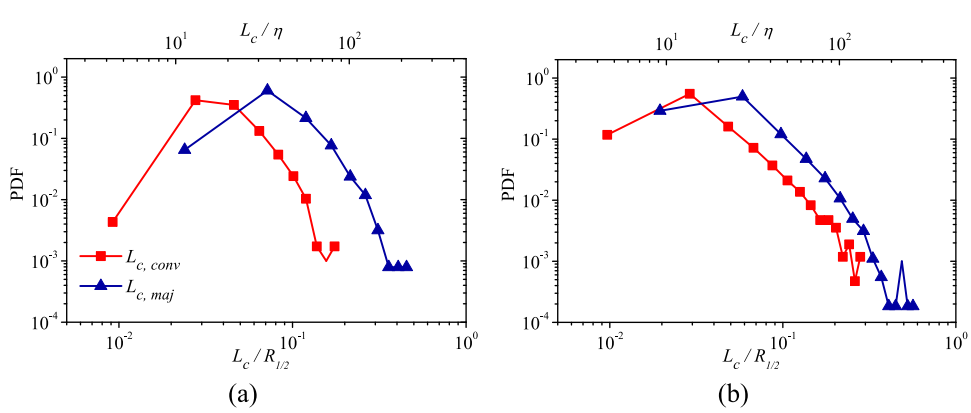

FIG. 12. PDF of length scale of droplet clusters at $R = 0$ mm for (a) $\phi_m = 0.01$ and (b) $\phi_m = 0.07$. The cluster length scales calculated using both the conventional method and current approach are shown.

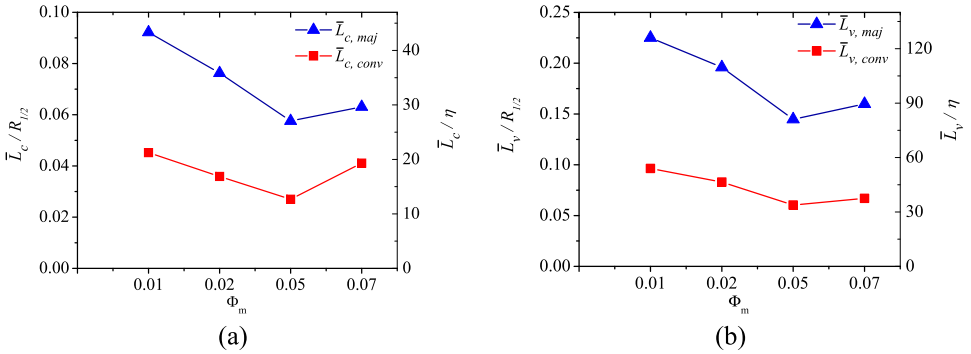

FIG. 13. Average length scale of (a) droplet clusters $\overline{L_c}$ and (b) voids $\overline{L_v}$ with respect to local liquid mass fraction ϕ_m at the measurement station $R = 0$ mm. The cluster length scales calculated using both the conventional method and current approach are shown.

First, $\overline{L_{maj}}$ is consistently smaller for higher local liquid mass fractions for both clusters and voids; however, the reduction of $\overline{L_{conv}}$ is not significant. The measurement of average length scales based on the conventional method is biased towards smaller cluster length scales and not much influenced within the current range of injector operating conditions. Second, notice that $\overline{L_{c,maj}}$ can be described either as a fraction of $R_{1/2}$ or multiples of tens of η. Hence, it is not straightforward to conclude if the large or small scale eddies mostly govern clustering of spray droplets. Nevertheless, it can be argued that clusters with $L_c \ll \overline{L_c}$ are under the influence of small scale eddies, while the large scale eddies influence clusters with $L_c \gg \overline{L_c}$, and as per Fig. 10, the variation of droplet concentration within a cluster can be significantly different depending on its size relative to the average size of all clusters. Next, one can notice in Fig. 13 that $\overline{L_{v,maj}}$ is always two to three times larger than $\overline{L_{c,maj}}$. This means that the voids are more influenced by large scale eddies in comparison to droplet clusters. Finally, the reduction in $\overline{L_{v,maj}}$ for higher ϕ_m indicates smaller length scales of large eddies, which is consistent with Table II that shows small but consistent reduction in $R_{1/2}$ for higher local droplet loading. On the other hand, for higher ϕ_m, the local Re_g is larger, which leads to smaller η. The droplets show poor response to small scale eddies since St_η is in the range of 5–20 (see Table II). Thus, the degree of clustering can be expected to be low at those scales. Hence, the above discussion implies that the reduction in $\overline{L_{c,maj}}$ for higher ϕ_m is due to smaller length scales of large eddies. This means stronger influence of large scale turbulent eddies on droplet cluster statistics in comparison to small scale ones. Our earlier study based on the measurement of average cluster length scale via D parameter (Manish and Sahu, 2019) also reported the same observation as in Fig. 13(a). However, the above result is in contrast to that of Sumbekova *et al.* (2017), who identified that L_c/η is proportional to Taylor Reynolds number and liquid volume fraction. The difference with respect to the present finding is possibly due to the fact that in the present case, (i) the flow is anisotropic and (ii) the droplet loading corresponds to the two-way coupling regime unlike the above study based on isotropic turbulence.

4. Discussion on multi-scale droplet clustering in the spray

The multi-scale droplet clustering in the spray as identified in the current experiments warrants further discussion on the physics behind such phenomena. Usually the mechanism responsible for preferential accumulation of particles heavier than the surrounding fluid is attributed to centrifuging of the particles out of the coherent eddies. In such cases, the particles accumulate in the low vorticity and highly strained region between successive eddies and the divergence of particle velocity field is non-zero in spite of the fluid flow being incompressible. This has been demonstrated by many research studies in the past (Squires and Eaton, 1990; Wang and Maxey, 1993; Fessler *et al.*, 1994; and Aliseda *et al.*, 2002, to name few). In those studies, the turbulence was homogeneous and isotropic and preferential particle accumulation was found to occur when the particle response time was of the order of the Kolmogorov time scale ($St_\eta \approx 1$). This means that the clustering was governed by the small scale eddies. However, later numerical studies on homogeneous and isotropic turbulence (for instance, Boffetta *et al.*, 2004) had shown that clustering is possible even when St_η is sufficiently larger than "one." In such cases, the particle response time introduces a characteristic scale in the inertial range so that clustering is not restricted to small scales and large scale inhomogeneity in particle concentration is produced. This was attributed to the "sweep-stick" mechanism, due to which particles cluster in a way that mimics the clustering of zero-acceleration points in the turbulent flow (Chen *et al.*, 2006; Goto and Vassilicos, 2008; and Coleman and Vassilicos, 2009). Although, for particles to "stick" to the low acceleration points, their relaxation time must be much smaller than the large eddy time scales.

In the present experiments with the air-assist sprays, (i) the St based on Kolmogorov scales was much greater than "one" (St_η was about 5 and 15 when based on AMD and SMD; this highlights the effect of polydispersity in the system). This means most of the droplets show poor response to the smallest eddies of the turbulent carrier flow and (ii) the length scale of droplet clusters varies over a wide range from multiples of η to about one-tenth of spray half-width. Also, the average cluster length scale ($\overline{L_c}$) is much larger (30–40 times) than η. Thus, the mechanism of droplet centrifuging out of small scale eddies that leads to preferential accumulation of droplets is not plausible. However, interestingly, $\overline{L_c}$ was found to be close to the Taylor length scale, λ (which is estimated from the dissipation rate). Also, St based on large eddies was about 0.1 and 0.3 when based on AMD and SMD, respectively, implying that most of the droplets have good response to the large scale eddies. These results support the sweep-stick mechanism of particle clustering. Sumbekova *et al.* (2017), in

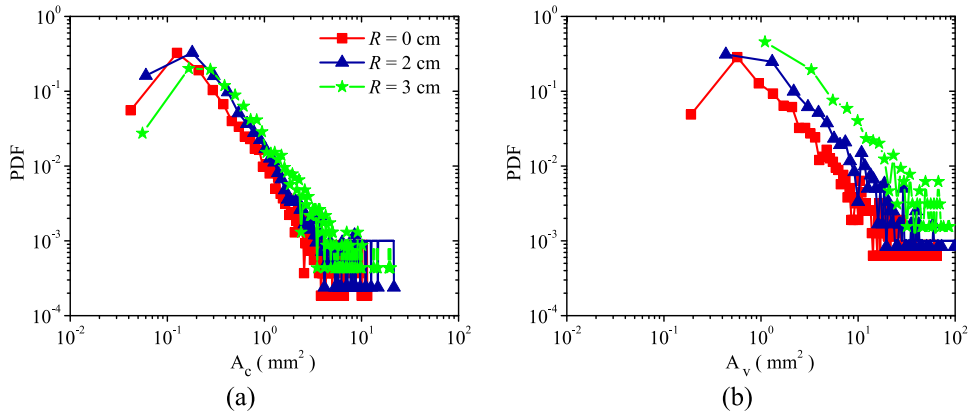

FIG. 14. PDF of (a) cluster area and (b) void area for ϕ_m = 0.07 at the three radial measurement stations 30 cm downstream of the injector exit.

their experiments on grid-generated isotropic turbulence, also attributed their observed multi-scale droplet clustering to the above mechanism. However, in contrast to their study, in the current experiments, the flow is anisotropic and also the cluster properties spatially vary across the spray.

C. Droplet clustering at different radial measurement stations

In this section, we discuss the tendency of droplets to cluster and the cluster characteristics for different radial measurement stations across the spray from the centre up to the boundary. Figure 14(a) presents the comparison of the PDFs of cluster areas for the three radial stations for ϕ_m = 0.07. Figure 14(b) shows the corresponding void area distributions. It is clearly observed that the void areas are larger towards the edge of the spray. This is in good agreement with the radial variation of large eddies in single phase turbulent jets for which the integral length scale increases away from the jet axis (Pope, 2001). This provides further evidence that the voids represent large eddies of the carrier phase turbulence. Though a similar trend is observed for clusters, the increase in cluster area appears relatively less significant. However, the normalized area distributions at the three stations nearly overlap with each other for both clusters and voids (not presented here). Similar results were obtained for other injector operating conditions. In conjunction with Figs. 8(b) and 9(b), the above finding further highlights the self-similarity of the droplet clustering process in the spray.

As mentioned earlier, the relative difference in the standard deviation of the Voronoi areas with respect to that for a RPP distribution, i.e., σ_{rel}, quantifies the degree of droplet clustering. Figure 15(a) plots the radial variation of σ_{rel} for the four injector operating conditions. The statistical uncertainty in the estimation of σ_{rel} was about ±0.3% with 95% confidence interval. Some important conclusions can be drawn from this figure. First, notice that σ_{rel} is positive for all cases, which confirms that non-random distribution of droplets (due to clustering) occurs across the spray. Next, in general, σ_{rel} is higher for higher liquid mass fractions for all radial measurement stations [also refer to Fig. 4(b)]. Thus, the degree of droplet clustering is proportional to local liquid mass loading, which is in good agreement with Sumbekova *et al.* (2017). Finally, for all injector operating conditions, σ_{rel} increases towards the spray boundary implying that the tendency of droplets to form clusters is higher. The above observation is further supported by the measurement of relative droplet number density (n_{rel}), which also quantifies the degree of droplet clustering. As shown in Fig. 15(b), the average relative droplet number density ($\overline{n}_{rel}$) increases away from the spray centre indicating stronger clustering. The statistical uncertainty in $\overline{n}_{rel}$ was around ±8%. However, not much difference in $\overline{n}_{rel}$ is observed for different ϕ_m at any measurement station. This is according to Fig. 10 which shows that the PDFs of n_{rel} for different ϕ_m nearly overlap with each other.

The reason behind the above observation can be attributed to the variation in the droplet's response to turbulent eddies across the spray. We note that Table II presents the droplet Stokes number *St* at the spray center. However, towards the spray boundary, the gas flow time scale is larger. This is because the length scale of the large scale eddies increases,

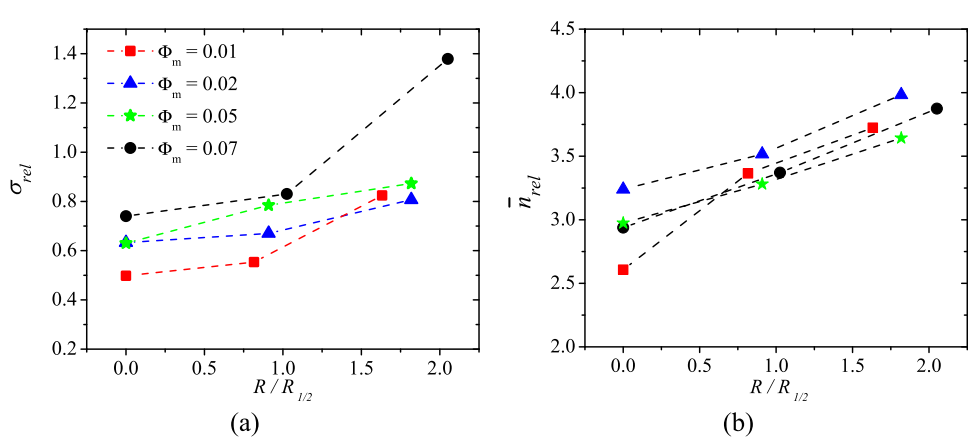

FIG. 15. Radial variation of (a) degree of droplet clustering σ_{rel} and (b) average relative droplet number density in clusters $\overline{n}_{rel}$ for different local liquid mass fractions, ϕ_m.

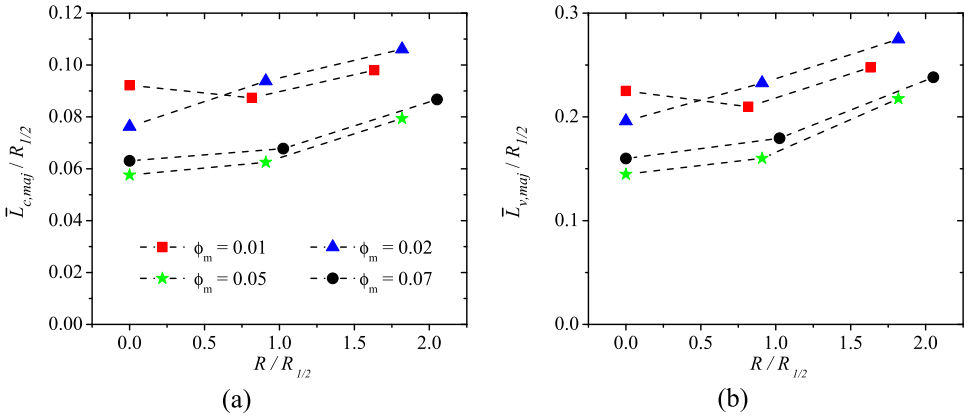

FIG. 16. Radial variation of (a) $\overline{L}_{c,maj}/R_{1/2}$ vs $R/R_{1/2}$ and (b) $\overline{L}_{v,maj}/R_{1/2}$ vs $R/R_{1/2}$ for all ϕ_m.

while the gas flow velocity fluctuations are smaller. Due to the same reason, the dissipation rate reduces, and so the time scale of the smallest eddies also increases. As a consequence, the response of a droplet to the gas flow turbulence improves radially away from the spray centre. Hence, the degree of clustering is higher. The measurement of D parameter for the current injector operating conditions in Manish and Sahu (2019) also showed similar results.

The average length scale of the droplet clusters and void areas measured at different radial stations are shown in Fig. 16. It can be observed that both $\overline{L}_{c,maj}$ and $\overline{L}_{v,maj}$ increase towards the spray edge. Though, not shown here, the average length scales following the conventional method, i.e., $\overline{L}_{conv}$ did not show much variation across the spray. Away from the central spray region, the average length scale of voids was found to increase, which is indicative of similar variation of large scale eddies. As mentioned earlier, this agrees well with the radial increase in the integral length scale of turbulence in a single phase turbulent jet. Since the response of droplets to turbulence also improves, the average length of droplet clusters is larger. This result is in good agreement with earlier studies (Heinlein and Fritsching, 2006; Sahu *et al.*, 2016; and Manish and Sahu, 2019). In addition, Fig. 16 shows that $\overline{L}_{c,maj}$ and $\overline{L}_{v,maj}$ are inversely proportional to ϕ_m for all measurement locations. Thus, the observation that the average length scale of large droplet clusters is smaller for higher local mass loading of droplets holds for all radial measurement stations across the spray.

While the mechanism responsible for the observed increase in the degree of clustering and reduction in cluster length scale for higher ϕ_m is not yet clear, we attempt to provide some discussion in that direction. As mentioned earlier, in the present experiments, the clustering of droplets mostly depends on two parameters, ϕ_m and Re_g (since St did not vary much for different injector operating conditions). Thus, the contribution of both ϕ_m and Re_g should be considered, which, though, cannot be varied independent of each other in the present case. Hence, the above observations can be attributed to (i) increase in intensity of clustering at inertial range since the local Re_g is also higher and (ii) two-way coupling effect, i.e., local turbulence modification due to rise in the local droplet number density (as a result of clustering) which in turn influences the gas-phase turbulence such that preferential accumulation of droplets is further promoted.

Finally, we note that the droplet clusters are three dimensional (3D) entities and two dimensional imaging of the 3D clusters can introduce some bias in the measurement of cluster length scale distribution. It is difficult to quantify this in the present experiments without performing 3D imaging of droplet clusters (for instance, tomographic imaging); however, accurate identification of droplets in such techniques is challenging. In addition we note that (i) in the present case, the cluster statistics are calculated considering a large number of image ensemble. Assuming that the 3D clusters would not have preferential orientation throughout their lifetime, this means the above statistics averages out the three dimensional effect. (ii) We have shown that at the present measurement locations (30 cm downstream of the injector exit, which is about 200 times the diameter of the injector exit), the characteristics of the spray jet are similar to those of a single phase turbulent jet. Since for such far downstream locations in a single phase turbulent jet the characteristics of radial and tangential components of velocity are nearly the same and the respective mean and fluctuations are smaller than those for the axial component of velocity (Pope, 2001), in the present experiments, we can expect that the component of gas phase velocity perpendicular to the laser sheet would not strongly contribute to droplet clustering in the same direction.

IV. CONCLUSIONS

Understanding the physics of clustering of polydispersed spray droplets is the aim of the current research work. For this purpose, measurement of individual clusters of droplets is vital rather than their statistics only. This was achieved by Voronoi analysis of the PIV images of the spray droplets far downstream of the exit of an air-assist injector. Experiments were performed for four different injector operating conditions to study the influence of local liquid mass fraction (ϕ_m), which was in the range 0.01–0.07 at the measurement locations. Droplet measurements were obtained for three radial measurement stations from the spray centre up to the boundary of the spray. The droplet size was measured using the ILIDS technique. The droplet Stokes number (St) based on the characteristic droplet size was about 0.05–0.3 when based on large eddies and 5–20 when based on Kolmogorov scales, which indicates partial and poor response of droplets to large and smallest eddies of the turbulent air flow around the droplets.

For higher ϕ_m, the local gas phase Re_g was higher although the St based on the characteristic droplet size did not vary much. The results are summarized as follows:

1. For all operating conditions and measurement locations, the areas of droplet clusters and voids were found to be distributed over a wide range, implying that droplet clustering in sprays is a multi-scale phenomenon. These results support the sweep-stick mechanism for preferential accumulation of droplets with $St_\eta > 1$ reported by earlier researchers. The normalized PDFs of cluster areas were nearly similar for all liquid mass loading and radial measurement stations across the spray. The same observations were found for the void areas. For both cluster and void area distributions, the algebraic decay exponent in the normalized PDFs was about −5/3. This suggests self-similarity in the droplet clustering process at the measurement locations.
2. The droplet number density in a cluster was always higher (up to ten times) than the average value measured across the image. An algebraic decay of the relative droplet number density (n_{rel}) in clusters with respect to cluster area (A_c) was found for $A_c < \overline{A_c}$; however, no such trends were present for $A_c > \overline{A_c}$. The PDFs of n_{rel} for different ϕ_m were nearly the same.
3. It was found that the conventional method of measurement of length scale of droplet clusters and voids (L_{conv}) as the square root of the respective areas leads to an underestimation since the corresponding PDFs are biased towards small scales. Instead, the length scale of a cluster/void was estimated by calculating the major axis of an ellipse (L_{maj}) of equivalent area and perimeter. $\overline{L_{conv}}$ was always smaller than $\overline{L_{maj}}$ for both clusters and voids. Also, no significant change in $\overline{L_{c,conv}}$ was observed either with different injector operating conditions or radial measurement stations in contrast to $\overline{L_{c,maj}}$.
4. The statistics of droplet clusters was found to strongly depend on ϕ_m and Re_g. The average cluster length $\overline{L_{c,maj}}$ was smaller and the degree of droplet clustering σ_{rel} was higher for higher local liquid mass fractions and Re_g for all measurement stations.
5. It was found that the characteristic size of clusters ($\overline{L_{c,maj}}$) can be interpreted either as a fraction of spray half-width or multiples of tens of the Kolmogorov scale. On this basis, it is difficult to conclude whether large or small scales of air flow turbulence mostly influence clustering of droplets. However, measurement of the characteristic size of voids (which was found to represent large scale turbulent eddies) and clusters for different ϕ_m and across the spray gave evidence of strong influence large scale eddies have on clustering.
6. The positive values of σ_{rel} for all cases emphasize a non-random distribution of polydispersed droplets due to clustering in spite of a wide range of droplet responses to different turbulent eddies. This was attributed to interaction of clusters due to some size class of droplets with droplets of other sizes which do not show the tendency for preferential accumulation. Due to better droplet response to carrier phase turbulence towards the edge of the spray, both σ_{rel} and n_{rel} increased towards the spray boundary implying higher degree of droplet clustering away from the spray center in the radial direction.

Akamatsu, F., Miutani, Y., Katsuki, M., Tsushima, S., and Cho, Y. D., "Measurement of the local group combustion number of droplet clusters in a premixed spray stream," Symp. (Int.) Combust. **26**, 1723–1729 (1996).

Aliseda, A., Cartellier, A., Hainaux, F., and Lasheras, J. C., "Effect of preferential concentration on the settling velocity of heavy particles in homogeneous isotropic turbulence," J. Fluid Mech. **468**, 77–105 (2002).

Andronov, L., Orlov, I., Lutz, Y., Vonesch, J.-L., and Klaholz, B. P., "Clustervisu, a method for clustering of protein complexes by Voronoi tessellation in super-resolution microscopy," Sci. Rep. **6**, 24084 (2016).

Attari, B., Weislogel, M., Wollman, A., Chen, Y., and Snyder, T., "Puddle jumping: Spontaneous ejection of large liquid droplets from hydrophobic surfaces during drop tower tests," Phys. Fluids **28**, 102104 (2016).

Balachandar, S. and Eaton, J. K., "Turbulent dispersed multiphase flow," Annu. Rev. Fluid Mech. **42**, 111–133 (2010).

Boffetta, G., De Lillo, F., and Gamba, A., "Large scale inhomogeneity of inertial particles in turbulent flows," Phys. Fluids **16**, L20–L23 (2004).

Boivin, M., Simonin, O., and Squires, K. D., "Direct numerical simulation of turbulence modulation by particles in isotropic turbulence," J. Fluid Mech. **375**, 235–263 (1998).

Calzavarini, E., Kerscher, M., Lohse, D., and Toschi, F., "Dimensionality and morphology of particle and bubble clusters in turbulent flow," J. Fluid Mech. **607**, 13–24 (2008).

Charalampous, G. and Hardalupas, Y., "Preferential concentration of water droplets in a volume of homogeneous and isotropic turbulence," in *49th AIAA Aerospace Sciences Meeting Including the New Horizons Forum and Aerospace Exposition* (AIAA, 2011), p. 791.

Chen, L., Goto, S., and Vassilicos, J., "Turbulent clustering of stagnation points and inertial particles," J. Fluid Mech. **553**, 143–154 (2006).

Chiu, H. and Liu, T., "Group combustion of liquid droplets," Combust. Sci. Technol. **17**, 127–142 (1977).

Coleman, S. and Vassilicos, J., "A unified sweep-stick mechanism to explain particle clustering in two-and three-dimensional homogeneous, isotropic turbulence," Phys. Fluids **21**, 113301 (2009).

Damaschke, N., Nobach, H., Nonn, T. I., Semidetnov, N., and Tropea, C., "Multi-dimensional particle sizing techniques," Exp. Fluids **39**, 336–350 (2005).

Elghobashi, S., "On predicting particle-laden turbulent flows," Appl. Sci. Res. **52**, 309–329 (1994).

Ferenc, J.-S. and Néda, Z., "On the size distribution of Poisson Voronoi cells," Physica A **385**, 518–526 (2007).

Ferrante, A. and Elghobashi, S., "On the physical mechanisms of two-way coupling in particle-laden isotropic turbulence," Phys. Fluids **15**, 315–329 (2003).

Fessler, J. R., Kulick, J. D., and Eaton, J. K., "Preferential concentration of heavy particles in a turbulent channel flow," Phys. Fluids **6**, 3742–3749 (1994).

Ficuciello, A., Blaisot, J., Richard, C., and Baillot, F., "Investigation of air-assisted sprays submitted to high frequency transverse acoustic fields: Droplet clustering," Phys. Fluids **29**, 067103 (2017).

Finotello, G., Padding, J. T., Deen, N. G., Jongsma, A., Innings, F., and Kuipers, J., "Effect of viscosity on droplet-droplet collisional interaction," Phys. Fluids **29**, 067102 (2017).

García-Villalba, M., Kidanemariam, A. G., and Uhlmann, M., "DNS of vertical plane channel flow with finite-size particles: Voronoi analysis, acceleration statistics and particle-conditioned averaging," Int. J. Multiphase Flow **46**, 54–74 (2012).

Glover, A., Skippon, S., and Boyle, R., "Interferometric laser imaging for droplet sizing: A method for droplet-size measurement in sparse spray systems," Appl. Opt. **34**, 8409–8421 (1995).

Goto, S. and Vassilicos, J., "Sweep-stick mechanism of heavy particle clustering in fluid turbulence," Phys. Rev. Lett. **100**, 054503 (2008).

Gounder, J. D., Kourmatzis, A., and Masri, A. R., "Turbulent piloted dilute spray flames: Flow fields and droplet dynamics," Combust. Flame **159**, 3372–3397 (2012).

Hardalupas, Y., Liu, C., and Whitelaw, J., "Experiments with disk stabilized kerosene-fuelled flames," Combust. Sci. Technol. **97**, 157–191 (1994).

Hardalupas, Y., Sahu, S., Taylor, A. M., and Zarogoulidis, K., "Simultaneous planar measurement of droplet velocity and size with gas phase velocities

in a spray by combined ILIDS and PIV techniques," Exp. Fluids **49**, 417–434 (2010).

Hardalupas, Y., Taylor, A., and Whitelaw, J. H., "Velocity and particle-flux characteristics of turbulent particle-laden jets," Proc. R. Soc. A **426**, 31–78 (1989).

Heinlein, J. and Fritsching, U., "Droplet clustering in sprays," Exp. Fluids **40**, 464–472 (2006).

Knowles, P. L. and Kiger, K. T., "Quantification of dispersed phase concentration using light sheet imaging methods," Exp. Fluids **52**, 697–708 (2012).

Lampa, A. and Fritsching, U., "Large eddy simulation of the spray formation in confinements," Int. J. Heat Fluid Flow **43**, 26–34 (2013).

Lian, H., "Droplet preferential concentration in homogeneous and isotropic turbulence," Ph.D. thesis, Imperial College London, 2014.

Longmire, E. K. and Eaton, J. K., "Structure of a particle-laden round jet," J. Fluid Mech. **236**, 217–257 (1992).

Maeda, M., Akasaka, Y., and Kawaguchi, T., "Improvements of the interferometric technique for simultaneous measurement of droplet size and velocity vector field and its application to a transient spray," Exp. Fluids **33**, 125–134 (2002).

Manish, M. and Sahu, S., "Analysis of droplet clustering in air-assist sprays using Voronoi diagrams," in *ICLASS 2018: 14th International Conference on Liquid Atomization and Spray Systems* (University of Illinois, Chicago, USA, 2018).

Manish, M. and Sahu, S., "Droplet clustering and local spray unsteadiness in air-assisted sprays," Exp. Therm. Fluid Sci. **100**, 89–103 (2019).

Maxey, M., "The gravitational settling of aerosol particles in homogeneous turbulence and random flow fields," J. Fluid Mech. **174**, 441–465 (1987).

McDonell, V., Adachi, M., and Samuelsen, G., "Structure of reacting and nonreacting swirling air-assisted sprays," Combust. Sci. Technol. **82**, 225–248 (1992).

Monchaux, R., "Measuring concentration with Voronoï diagrams: The study of possible biases," New J. Phys. **14**, 095013 (2012).

Monchaux, R., Bourgoin, M., and Cartellier, A., "Preferential concentration of heavy particles: A Voronoï analysis," Phys. Fluids **22**, 103304 (2010).

Monchaux, R., Bourgoin, M., and Cartellier, A., "Analyzing preferential concentration and clustering of inertial particles in turbulence," Int. J. Multiphase Flow **40**, 1–18 (2012).

Nilsen, C., Andersson, H. I., and Zhao, L., "A Voronoï analysis of preferential concentration in a vertical channel flow," Phys. Fluids **25**, 115108 (2013).

Obligado, M., Cartellier, A., and Bourgoin, M., "Experimental detection of superclusters of water droplets in homogeneous isotropic turbulence," Europhys. Lett. **112**, 54004 (2015).

Obligado, M., Missaoui, M., Monchaux, R., Cartellier, A., and Bourgoin, M., "Reynolds number influence on preferential concentration of heavy particles in turbulent flows," J. Phys.: Conf. Ser. **318**, 052015 (2011).

Obligado, M., Teitelbaum, T., Cartellier, A., Mininni, P., and Bourgoin, M., "Preferential concentration of heavy particles in turbulence," J. Turbul. **15**, 293–310 (2014).

Pope, S. B., *Turbulent Flows* (Cambridge University Press, 2001).

Rabencov, B. and van Hout, R., "Voronoi analysis of beads suspended in a turbulent square channel flow," Int. J. Multiphase Flow **68**, 10–13 (2015).

Razzaghi, A., Banitabaei, S., and Amirfazli, A., "Shedding of multiple sessile droplets by an airflow," Phys. Fluids **30**, 087104 (2018).

Sahu, S., "Experimental study of isothermal and evaporative sprays," Ph.D. thesis, Imperial College London, 2011.

Sahu, S., Hardalupas, Y., and Taylor, A., "Droplet–turbulence interaction in a confined polydispersed spray: Effect of droplet size and flow length scales on spatial droplet–gas velocity correlations," J. Fluid Mech. **741**, 98–138 (2014).

Sahu, S., Hardalupas, Y., and Taylor, A., "Droplet–turbulence interaction in a confined polydispersed spray: Effect of turbulence on droplet dispersion," J. Fluid Mech. **794**, 267–309 (2016).

Sahu, S., Hardalupas, Y., and Taylor, A., "Interaction of droplet dispersion and evaporation in a polydispersed spray," J. Fluid Mech. **846**, 37–81 (2018a).

Sahu, S., Manish, M., and Hardalupas, Y., "Two-phase characterization for turbulent dispersion of sprays: A review of optical techniques," in *Droplets and Sprays: Applications for Combustion and Propulsion*, edited by Basu, S., Agarwal, A. K., Mukhopadhyay, A., and Patel, C. (Springer Singapore, Singapore, 2018b), pp. 247–273.

Saw, E. W., Shaw, R. A., Ayyalasomayajula, S., Chuang, P. Y., and Gylfason, Á., "Inertial clustering of particles in high-Reynolds-number turbulence," Phys. Rev. Lett. **100**, 214501 (2008).

Scott, S. J., Karnik, A. U., and Shrimpton, J. S., "On the quantification of preferential accumulation," Int. J. Heat Fluid Flow **30**, 789–795 (2009).

Shaw, R., Kostinski, A., and Larsen, M., "Towards quantifying droplet clustering in clouds," Q. J. R. Meteorol. Soc. **128**, 1043–1057 (2002).

Smith, N., Nathan, G., Zhang, D., and Nobes, D., "The significance of particle clustering in pulverized coal flames," Proc. Combust. Inst. **29**, 797–804 (2002).

Soldati, A. and Marchioli, C., "Sediment transport in steady turbulent boundary layers: Potentials, limitations, and perspectives for Lagrangian tracking in DNS and LES," Adv. Water Resour. **48**, 18–30 (2012).

Sornek, R. J. and Dobashi, R., "Effect of turbulence on spatial distribution and group behavior of droplet in a spray flame," Combust. Sci. Technol. **161**, 191–211 (2000).

Squires, K. D. and Eaton, J. K., "Particle response and turbulence modification in isotropic turbulence," Phys. Fluids A **2**, 1191–1203 (1990).

Sumbekova, S., Cartellier, A., Aliseda, A., and Bourgoin, M., "Preferential concentration of inertial sub-Kolmogorov particles: The roles of mass loading of particles, Stokes numbers, and Reynolds numbers," Phys. Rev. Fluids **2**, 024302 (2017).

Sundaram, S. and Collins, L. R., "A numerical study of the modulation of isotropic turbulence by suspended particles," J. Fluid Mech. **379**, 105–143 (1999).

Tagawa, Y., Roghair, I., Prakash, V. N., van Sint Annaland, M., Kuipers, H., Sun, C., and Lohse, D., "The clustering morphology of freely rising deformable bubbles," J. Fluid Mech. **721**, R2-1–R2-13 (2013).

Tennekes, H. and Lumley, J. L., *A First Course in Turbulence* (MIT Press, 1972).

Tropea, C., "Optical particle characterization in flows," Annu. Rev. Fluid Mech. **43**, 399–426 (2011).

Wang, L.-P. and Maxey, M. R., "Settling velocity and concentration distribution of heavy particles in homogeneous isotropic turbulence," J. Fluid Mech. **256**, 27–68 (1993).

Wood, A., Hwang, W., and Eaton, J., "Preferential concentration of particles in homogeneous and isotropic turbulence," Int. J. Multiphase Flow **31**, 1220–1230 (2005).

Yang, T. and Shy, S., "Two-way interaction between solid particles and homogeneous air turbulence: Particle settling rate and turbulence modification measurements," J. Fluid Mech. **526**, 171–216 (2005).

Yang, X. and Turan, A., "Simulation of liquid jet atomization coupled with forced perturbation," Phys. Fluids **29**, 022103 (2017).

Zimmer, L. and Ikeda, Y., "Simultaneous laser-induced fluorescence and mie scattering for droplet cluster measurements," AIAA J. **41**, 2170–2178 (2003).